Q. J. R. Meteorol. Soc. (1998), **124**, pp. 2771–2792

A novel approach to atmospheric dispersion modelling: The Puff–Particle Model

By PETER DE HAAN* and MATHIAS W. ROTACH
Swiss Federal Institute of Technology, Switzerland

(Received 21 January 1997; revised 19 May 1998)

SUMMARY

The Puff–Particle Model (PPM) uses a new approach to problems of three-dimensional atmospheric dispersion from micro- to mesoscale. The pollutant particles are grouped in clusters treated as Gaussian puffs, which are dispersed making use of the concept of relative diffusion. The centre of mass of each puff is moved along a stochastic trajectory. This trajectory is derived from particle trajectories given by a Lagrangian stochastic-dispersion model. In this way, the PPM retains the advantages of traditional puff models and those of particle models, and is able to take into account the correct probability density function of the stochastic velocity components. The effect of meandering (caused by turbulent eddies larger than the puff but not resolved by the flow field) is simulated by the puff centre trajectories, yielding a complete description of dispersion. The PPM is validated using measurements from three tracer experiments in Copenhagen, Lillestrøm and Kincaid.

KEYWORDS: Lagrangian dispersion Model validation Particle model Puff model Relative diffusion

1. INTRODUCTION

Particle models (or random-flight models) are generally accepted to be most appropriate to describe dispersion from passive non-buoyant releases in inhomogeneous turbulence (Wilson and Sawford 1996). In particular, dispersion in the convective boundary layer is successfully modelled using this approach (e.g. Luhar and Britter 1989; Hurley and Physick 1993; Rotach *et al.* 1996). According to the underlying theory they yield ensemble plume statistics, i.e. absolute dispersion. The major disadvantage of this model type is its excessive consumption of computing time. Puff models are much faster (and thus less computing time demanding) than particle models, but still allow for simulating dispersion in inhomogeneous turbulence. Furthermore, when using relative dispersion to grow the puffs, this approach is suited to modelling instantaneous releases (one single realisation of a plume). This quality makes them useful for predicting concentration fields in cases of hazardous releases of toxic material (Mikkelsen and Larsen 1984). On the other hand, when being used in conjunction with absolute dispersion, puff models yield ensemble plume statistics. Since the shape of the puffs is often assumed to be Gaussian, these predictions might be less accurate than those of particle models, especially for non-Gaussian turbulence (convective conditions), but again, they are 'cheaper' in terms of computing time. As additional advantages over particle models, puff models allow for a reasonable description of the effects of buoyant emissions (plume rise) and might even allow for treating chemical reactions within the puffs.

The Puff–Particle Model (PPM) attempts to combine the advantages of both these model types. As a 'generic puff model' it is able to predict instantaneous statistics but it uses the information of its 'particle part' to describe the trajectories of the puffs, thus assuring an optimal representation of the dispersion process even under convective conditions.

Hurley (1994) has proposed a model 'Partpuff' which goes in the same direction as the PPM, but is based on a different concept. Essentially, he uses a one-dimensional particle model to describe the vertical dispersion while assuming a horizontal dispersion of Gaussian shape. Another model, the RAPTAD (Random Particle Transport and Diffusion) model of Yamada and Bunker (1988), combines a particle model with absolutely dispersed Gaussian puffs. This approach is compared to the PPM in more detail in section 3.

* Corresponding author: Swiss Federal Institute of Technology, GIETH, Winterthurerstrasse 190, 8057 Zurich, Switzerland. e-mail: dehaan@geo.umnw.ethz.ch.

The principles of the PPM were first described in de Haan and Rotach (1995). Here, a full description is provided (section 2), several improvements of the original concept are presented (section 3) and the model is extensively validated against tracer data (section 4).

2. Principles of the PPM

(*a*) *The concept*

In short, puff models simulate the dispersion of a 'cluster of pollutant particles', which is released as an entity, by following it along a trajectory and continuously increasing the puff's dimensions. Basically, it can be distinguished between two different approaches:

- If the puff model aims at identifying the puff with an individual, physically realistic cluster of particles, the concept of relative dispersion (i.e. 2-particle statistics, Borgas and Sawford 1994) has to be used. This concept takes into account that eddies smaller than the actual puff size will contribute to its growth, while larger eddies move the puff as a whole (Fig. 1). Relative dispersion accounts for the dispersion of a cluster with respect to the centre of mass of the cluster. This way, the dispersion of a single plume is described correctly.
- If the puff model has the goal to predict the dispersion of an ensemble of plumes, rather than a single plume, absolute dispersion should be used to describe the growth of the puffs. These puffs do not correspond to any cluster in nature. They are an average over many realisations of individual clusters. Most formulations in the literature of absolute dispersion correspond to a plume-averaging time of roughly one hour, corresponding to the spectral gap between synoptic and turbulent frequencies. Absolute dispersion then gives an estimate of the mean dispersion of a plume averaged over one hour, which is the combined effect of relative diffusion and of the meandering of the puff respective to a fixed point, caused by eddies larger than the puff.

This means that puff models using *absolute dispersion* are able to predict ensemble plume concentrations. They are not suited to give correct concentration predictions for instantaneous releases (systematically overpredicting dispersion and hence underpredicting concentrations). For the latter case, relative diffusion should be used. When using *relative diffusion* in puff models, the predicted spread of a puff resembles the spread of one single pollutant cluster, but no prediction can be made about the amount of meandering of the trajectory of such a single cluster. However, for near-field predictions, the dispersing effect of meandering should be taken into account, since otherwise concentrations might be overpredicted.

When modelling instantaneous releases, flow fields may often be available for several times during one hour. However, the use of absolute dispersion can only be justified if the time, T, between the succeeding flow fields available to the dispersion model is at least

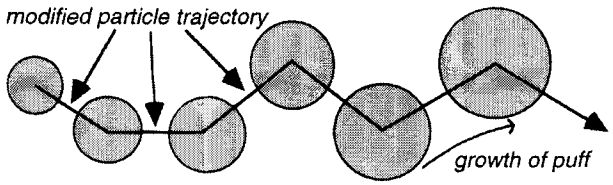

Figure 1. The Puff–Particle Model groups pollutant particles together in puffs, whose centres of mass are moved along particle trajectories calculated by a stochastic particle model.

roughly 30 min. If T becomes smaller, an increasing range of turbulent eddies will be resolved by the flow fields. Their dispersing effect is also included in absolute dispersion, leading to overestimated total dispersion. One way to circumvent this problem would be to adjust the turbulence parameters σ_u, σ_v and σ_w that are used to determine the rate of growth of the puffs so they correspond to T.

If, on the other hand, relative diffusion together with frequently updated flow fields are used, there will generally be a 'gap of dispersion' not covered by the flow fields nor by the relative dispersion. This gap will be largest in the beginning when the puff is small, and vanishes later on when the size of the puff reaches the order of $\bar{u}T$, where $\bar{u}$ is a representative mean wind speed.

In practice it is difficult (or at least computationally very expensive) to provide the flow field at a sufficiently high temporal rate. For example, Thykier-Nielsen *et al.* (1994) use three ten-minute intervals to simulate the low-frequency contribution to the puff movement over a period of half an hour.

In the PPM the concept of relative diffusion is used to describe the spread of individual puffs as in other puff models (Mikkelsen and Larsen 1984; Thykier-Nielsen *et al.* 1989). The 'gap' in the description of dispersion is 'filled in' by artificially generating the meandering of the puffs' centres of mass. These meandering trajectories aim at simulating the meandering effect of all those eddies not resolved by the flow field but still larger than the puff. These trajectories of the puffs' centres of mass are determined from 'particle trajectories' as obtained from a stochastic particle-dispersion model (Fig. 1). This concept has several advantages:

- The puff-particle approach gives a realistic picture of the transport (caused by the mean wind, and provided by the flow field updates), the amount of meandering (covered by the stochastic puff centre trajectories) and the diffusion of the release itself (caused by eddies smaller than the size of the puff, and taken into account by relative diffusion). The amount of meandering which has to be simulated by the puff centre trajectories depends on T.
- For the computation of ensemble plume statistics (absolute dispersion), an average is taken over many of such single meandering plume realisations. The 'particle-part' of the PPM thus fills the 'gap' (if there is one) in dispersion caused by the spectral gap between the range of eddies resolved by the flow field and those covered by relative diffusion.
- It is possible to have only one flow field computation, which may even be determined from parametrized flow and turbulence profiles in horizontally homogeneous conditions. In this case, T is set equal to the total averaging time for the concentration measurements, normally equal to the total duration of the experiment to be simulated.
- Dispersion in convective boundary layers can be simulated realistically with the PPM. With conventional puff models reasonable results are difficult to obtain unless a highly sophisticated model (e.g. Large-Eddy Simulation) is used to produce the meteorological information (which, in turn, makes it unnecessary to use any dispersion model).

The 'particle part' of the PPM accounts for the effects of eddies larger than the actual puff size, which move the puff as a whole (meandering). In consequence, the cycling frequencies represented by this meandering must correspond to the turbulent eddies to be simulated, i.e. the low-frequency part of the energy spectrum. This is done by defining a threshold frequency, n^*, changing with puff size, i.e. travel time. With increasing puff

size, large parts of the turbulent fluctuations will have to be eliminated from the particle trajectories, when using them as puff centre trajectories, in the particle part of the PPM (low-pass filter). Eventually, this allows for 'turning off' the particle part when the puff size has reached a certain extent (see section 3). Since absolute dispersion as simulated by stochastic particle models is not an explicit function of T, but only assumes that T is in the so-called 'spectral gap', no high-pass filter is used in the PPM. This would be necessary for T smaller than approximately 15 min.

Two possible interpretations can be given for the concept of the PPM. Firstly, it can be viewed as a modified puff model, in which the dispersion is described correctly, since the effect of all eddies not resolved by the flow field is simulated using the particle part of the PPM. On the other hand, the PPM may be considered a method to speed up a true particle model by combining each, say, 100 particles into one puff, thereby saving considerable computing time. Due to the additional calculation of the dispersion of the puffs, puff splitting schemes etc., the PPM is approximately twenty times faster than a comparable particle model.

(*b*) *The puff part of the PPM*

In the PPM, all pollutants are described as clusters of particles and are approximated by three-dimensional Gaussian puffs. With the puff–particle approach, the dispersing effect of the turbulent eddies smaller than the puff itself are taken into account by the puff part of the model, whereas the effect of the large eddies is simulated by the particle part. Within the statistical approach to describe dispersion of passive scalars, a distinction must be made between the dispersion of particles relative to a fixed coordinate system (absolute dispersion) and the spread of a cluster of particles (relative diffusion). One of the first to point out this fundamental difference was Richardson (1926). The first approach treats every particle as being independent (1-particle statistics) and thus can only describe absolute dispersion of the plume. To describe the effects of relative diffusion, 2-particle statistics must be used (see e.g. Borgas and Sawford 1994, for a review). During its growth, a cluster of particles is affected by an increasing range of turbulent eddies, since larger and larger eddies will be capable of separating two particles from each other as puff sizes grow. On the other hand, within the framework of absolute dispersion, turbulent eddies of all sizes are capable of influencing the distance of a single particle from its point of release, thus enhancing the plume dimensions.

To identify the cluster, marked passive particles with an absolute velocity u within the fluid are followed, released at a time $t = 0$. The spread, σ, of such a cluster at subsequent times is defined as:

$$\sigma^2(t) = \overline{\left\langle \left\{ \int_0^t v(\tau)\, \mathrm{d}\tau \right\}^2 \right\rangle}, \tag{1}$$

where the integration runs along a Lagrangian orbit $v = u - V_{\mathrm{cm}}$, and the velocity of the centre of mass of the cluster is denoted by V_{cm}. The overbar in Eq. (1) and subsequently up to section 2(d) denotes the average over all the particles within the puff, and the angular brackets throughout refer to an ensemble average. Mikkelsen *et al.* (1987) use a kinematic–statistical model in which the rate of growth (Batchelor 1952; Smith and Hay 1961) of the puff:

$$\frac{\mathrm{d}\sigma^2}{\mathrm{d}t} = 2 \int_0^t \overline{\langle v(t)v(t-\tau)\rangle}\, \mathrm{d}\tau, \tag{2}$$

is related to one-dimensional velocity spectra. They assume that the stochastic displacements of the particles obey independent and identical Gaussian statistics, thus leading to clusters of particles (i.e. puffs) being of Gaussian shape.

Batchelor (1952) distinguishes 'near-field', 'intermediate range' and 'far-field' approximate solutions to Eq. (2). In the initial phase of spread of the puff, the initial size of the puff, σ_0, is an important parameter. For travel times $t < \{\sigma_0^2/\overline{\langle v^2(0)\rangle}\}^{1/2}$, he gives as the near-field approximation:

$$\sigma_{\mathrm{nf}}^2(t) = \sigma_0^2 + \overline{\langle v^2(0)\rangle} t^2. \tag{3}$$

For the 'intermediate' time interval, when viscosity and the initial puff size are no longer dominant parameters, but before the Lagrangian integral time-scale T_{L} becomes an important scaling parameter (i.e. for times corresponding to a frequency in the inertial subrange), the intermediate-field approximation is:

$$\sigma_{\mathrm{if}}^2(t) = C\varepsilon t^3, \tag{4}$$

where ε denotes the dissipation rate of turbulent kinetic energy. Mikkelsen *et al.* (1987) relate Eq. (4) to the universal constant of the Lagrangian structure function, C_0, as $\sigma^2(t) = \frac{1}{3}C_0\varepsilon t^3$. Recent estimates for C_0 indicate that $C_0 = 3.0 \pm 0.5$ (Du *et al.* 1995; Rotach 1995), so that the corresponding value of C in Eq. (4) has been chosen equal to unity in the present work.

For $t > T_{\mathrm{L}}$, Eq. (2) reduces to the description of single-particle dispersion in the far-field limit (Taylor 1921), thus leading to the far-field formulation:

$$\sigma_{\mathrm{ff}}^2(t) = 2\langle u^2\rangle T_{\mathrm{L}} t. \tag{5}$$

Evaluating $\overline{\langle v^2(0)\rangle}$ from Eq. (3) is not trivial. If the initial fluctuating velocity components of the particles within the puff originate from a three-dimensional Gaussian distribution (leading to $\vec{V}_{\mathrm{cm}}(0) = \vec{0}$ for the cluster):

$$\overline{\langle v^2(0)\rangle} = r_1^{\mathrm{E}}\langle u'^2(0)\rangle + r_2^{\mathrm{E}}\langle v'^2(0)\rangle + r_3^{\mathrm{E}}\langle w'^2(0)\rangle, \tag{6}$$

with the velocity variances being evaluated at $t = 0$. Here, $\langle u'^2(0)\rangle$, $\langle v'^2(0)\rangle$ and $\langle w'^2(0)\rangle$ denote the variances corresponding to this Gaussian distribution, and are equal to the variances of the longitudinal, lateral and vertical turbulent velocities, respectively, at the point of release. Equation (6) does not depend on the correlation coefficient $\rho = \langle u'w'\rangle/(\langle u'^2\rangle\langle w'^2\rangle)$ of the distribution. Recall that v denotes the absolute velocity relative to the puff's centre, whereas the u_i' refer to the fixed coordinate system with the u-axis parallel to the direction of the mean wind.

The three terms $r_i^{\mathrm{E}}(i = 1, 2, 3)$ in Eq. (6) range from zero for point releases to unity for very large source sizes. They indicate what amount of the total kinetic energy is represented by eddies smaller than the initial source size. The superscript E denotes that they depend on the Eulerian turbulent velocity spectra at the point of release. The definition of these ratios is given in section 3, where ratios depending on Lagrangian spectra are also investigated.

In atmospheric dispersion modelling with Gaussian puffs, which are characterized by the values of the three standard deviations, s_i $(i = 1, 2, 3)$ for the longitudinal, lateral and vertical direction, respectively, σ^2 in Eqs. (1) to (5) can be replaced by s_i^2 if $\overline{\langle v^2(0)\rangle}$ is replaced by $\langle u_i^2(0)\rangle$ and $\langle u^2\rangle$ by $\langle u_i^2\rangle$ (Eq. 5), where $(u_1, u_2, u_3) = (u', v', w')$.

In the PPM, Eqs. (3), (4) and (5) are used to describe the growth of puffs for small, intermediate and large travel times, respectively. These equations give puff standard deviations as a function of t. In Lagrangian particle models, t is not normally known (and causes problems after furcation of puffs where the puff dimensions become smaller, see below). Therefore, the pseudo-time method, which is frequently used in Lagrangian puff

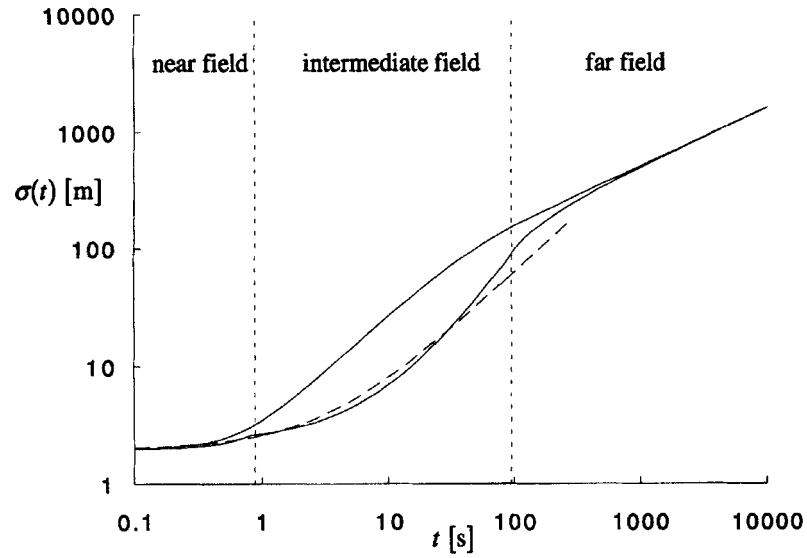

Figure 2. Puff spread σ (as defined by Eq. 1) as a function of travel time t. The upper solid line is calculated from Taylor's (1921) single-particle diffusion theory, $0.5\,\mathrm{d}\sigma^2/\mathrm{d}t = \overline{\langle u^2\rangle} t_a(t)$, where $t_a(t) = \int_0^t \exp(-\xi/T_L)\,\mathrm{d}\xi$ is assumed and an initial source size $\sigma_0 = 2$ m was adopted. The lower solid line shows the integration of Eqs. (3), (4) and (5), where the vertical dotted lines mark the change between them. Also shown (dashed line) is the puff formula of Pasquill and Smith (1983), $\sigma_{\max} = \sigma_0 + \alpha \overline{\langle u^2\rangle}^{1/2} t$, with the re-evaluated value $\alpha = 0.30$. See text for definitions and further explanation.

models (e.g. Scire *et al.* 1995), is applied to Eqs. (3) to (5). At the beginning of time step $t' = t + \Delta t$, with the spread σ_t of the puff at time t, we calculate a pseudo-time $\tau = f(\sigma_t)$ using Eqs. (3), (4) or (5). Then, we evaluate $\sigma_{t+1} = \sigma(t + \Delta t)$. This scheme allows for inhomogeneous and nonstationary turbulence conditions. When a puff travels from a region with a low-turbulence level into a region with high turbulence, its pseudo-time will change. This change in pseudo-time reflects the fact that the turbulence spectrum at the new location has changed, i.e. the rate of growth, depending on the turbulent kinetic energy of those eddies being small enough to disperse the puff, has increased. For T_L, the estimates of Gryning *et al.* (1987) are adopted.

Figure 2 shows the resulting puff size under modestly convective conditions. Since Eq. (3) is valid for $t < \{\sigma_0^2/\overline{\langle v^2(0)\rangle}\}^{1/2}$, the transition from the near-field to the intermediate-field approximation is assumed at a threshold time $t_1 = c_1\{\sigma_0^2/\overline{\langle v^2(0)\rangle}\}^{1/2}$, with $c_1 = 0.5$. The transition from the intermediate-field to the far-field formulation is assumed to take place as soon as $\mathrm{d}\sigma/\mathrm{d}t$ from Eqs. (4) and (5) become equal, i.e. at $t_2 = (1/3)\sqrt{(2\langle u^2\rangle T_L)/\varepsilon}$. Figure 2 shows that the difference in puff dimensions from absolute and relative diffusion is largest in the intermediate field. The approximation of Pasquill and Smith (1983, pp. 230–232; dashed line in our Fig. 2) is valid for near-field and intermediate-field travel times only, since it does not approach the Taylor (1921) limit (Eq. (5)).

The initial standard deviations of the puff's normal distribution equal the radius of the source. All emitted puffs carry an initial mass such that the sum of the puffs which are emitted per unit time equals the emission rate of the source. During a simulation time step of, say, 1 second, the centres of mass of the puffs are moved along a trajectory derived from particle trajectories (see section 3). Based on the new position and the travel distance, new puff dimensions σ_1 are calculated. Furthermore, an option allows for puffs to be split up

into several new puffs, for example after exceeding the grid size of the wind field in either direction. This mass-consistent procedure is called furcation, and its implementation in the PPM is a modified version of the procedure of Thykier-Nielsen *et al.* (1989). In the PPM, a trifurcation is applied in the vertical direction and a pentafurcation (the original puff is replaced by five new puffs) in the horizontal plane. The new puffs have half the size of, and are placed half a standard deviation apart from, the original puff; also one new puff is placed at the original location itself. The masses of the new puffs are chosen such that the new total density distribution (of the three or five furcated puffs) is as similar as possible to the distribution of the original puff.

Any location within the three-dimensional domain can be specified as a 'receptor'. This procedure, based on time steps of 1 second, is repeated until the pollutant concentrations have reached a quasi-steady state at the receptor point most distant from the source. Typically, the trajectories of about 1000 puffs are followed to model three-dimensional concentration patterns.

(*c*) *The stochastic-dispersion model*

To move the centres of mass of the puffs, in principle any particle model can be used. In the PPM, a three-dimensional Lagrangian stochastic-dispersion model is used that fulfills the well-mixed condition for neutral to convective conditions. It is based on a model described in Rotach *et al.* (1996) but is expanded to three dimensions. This model allows for a continuous transition between correlated Gaussian turbulence on the one hand, and uncorrelated skewed turbulence on the other, of which the latter is characteristic of the convective boundary layer. The evolution of velocity $\vec{\mathbf{u}}$ and position $\vec{\mathbf{x}}$ of tracer particles is described by the stochastic differential equations $\mathrm{d}u_i = a_i(\vec{\mathbf{x}}, \vec{\mathbf{u}}, t)\,\mathrm{d}t + b_{ij}\mathrm{d}\xi_j$ so that $\mathrm{d}\vec{\mathbf{x}} = \vec{\mathbf{u}}\,\mathrm{d}t$. The $\mathrm{d}\xi_i$ must be a Wiener process with zero mean, and variance $\mathrm{d}t$. The well-mixed criterion (Thomson 1987) requires that the probability density function (pdf) of the particle velocities, $P_{2\mathrm{d}}$, fulfills the Fokker–Planck equation:

$$\frac{\partial}{\partial t}P_{2\mathrm{d}} = -\frac{\partial}{\partial x_i}(u_i P_{2\mathrm{d}}) - \frac{\partial}{\partial u_i}(a_i P_{2\mathrm{d}}) + \frac{\partial^2}{\partial u_i \partial u_j}(B_{ij} P_{2\mathrm{d}}) \tag{7}$$

where $2B_{ij} = b_{ik}b_{jk}$. Equation (7) is used to derive the functions a_i and b_i (see Rotach *et al.* 1996 for details). For stationary turbulence it can be written:

$$a_i P_{2\mathrm{d}} = \frac{\partial}{\partial u_j}(B_{ij} P_{2\mathrm{d}}) + \Phi_i, \tag{8}$$

where Φ_i obeys:

$$\frac{\partial}{\partial u_i}\Phi_i = -\frac{\partial}{\partial x_i}(u_i P_{2\mathrm{d}}), \tag{9}$$

with the restriction on Φ_i that $\Phi_i \to 0$ for $|\vec{\mathbf{u}}| \to \infty$.

The particle model of Rotach *et al.* (1996) is constructed from a two-dimensional pdf $P_{2\mathrm{d}}$:

$$P_{2\mathrm{d}} = f P_u P_c + (1 - f) P_{\mathrm{g}} \tag{10}$$

where P_c is a one-dimensional skewed pdf for the vertical velocity (Luhar and Britter 1989). P_u is a one-dimensional Gaussian distribution of the horizontal longitudinal velocity component, P_{g} is a two-dimensional jointly Gaussian distribution for u' and w' and f is a transition function. If $f = 1$, the total pdf becomes equal to $P_u \cdot P_c$ (i.e. the velocity components are uncorrelated, w is skewed). On the other hand, if $f = 0$, u' and w' are jointly

Gaussian distributed. From this pdf the model for the velocity increments is constructed in the usual manner (see e.g. Thomson 1987).

The transition function f is formulated in such a way that for large w_* (the convective velocity scale) f becomes unity throughout most of the boundary layer, and equals zero over large parts of a neutral or stable boundary layer ($w_* = 0$). Thus, it is assumed that the transitions from a Gaussian to a skewed distribution in w' and from correlated to uncorrelated velocity fluctuations (u', w') are occurring at the same rate, governed by the transition function f, as stability changes. For more details about f see Rotach *et al.* (1996).

To extend the above model to three dimensions, the lateral velocity fluctuations, v', are assumed to be fully independent of the other fluctuations, with a Gaussian pdf. Thus, the three dimensional total pdf is constructed through $P_{\text{tot}} = P_{2\text{d}} P_v$, where P_v is the Gaussian distribution of the lateral velocity component. The three-dimensional model is again constructed according to the constraints outlined by Thomson (1987). This requires for horizontally homogeneous conditions:

$$\frac{\partial}{\partial u_i}\Phi_i = -\frac{\partial}{\partial z}(w' P_{2\text{d}} \cdot P_v). \tag{11}$$

In order to retain the formulations of the two-dimensional model, we take $\Phi_u^{2\text{d}}$ and $\Phi_w^{2\text{d}}$, which fulfill:

$$\frac{\partial}{\partial u}\Phi_u^{2\text{d}} + \frac{\partial}{\partial w}\Phi_w^{2\text{d}} = -\frac{\partial}{\partial z}(w' P_{2\text{d}}). \tag{12}$$

On defining $\Phi_u = \Phi_u^{2\text{d}} \cdot P_v$ and $\Phi_w = \Phi_w^{2\text{d}} \cdot P_v$, this leads to:

$$\frac{\partial}{\partial v}\Phi_v = -w' P_{2\text{d}} \frac{\partial}{\partial z}(P_v), \tag{13}$$

so that:

$$\Phi_v(v') - \Phi_{v'=-\infty} = -w' P_{2\text{d}} \int_{-\infty}^{v'} \left(\frac{\partial}{\partial z} P_v\right) \mathrm{d}v, \tag{14}$$

where the second term on the left-hand side of Eq. (14) equals zero. The solution of this integral is straightforward and the final result is:

$$\Phi_v = w' \cdot P_{2\text{d}} v' P_v \frac{1}{\sigma_v} \frac{\partial \sigma_v}{\partial z}, \tag{15}$$

where σ_v is the standard deviation of the lateral velocity component in P_v.

(*d*) *Parametrization of turbulence statistics*

In principle, the PPM can be driven with any kind of meteorological input. If no measurements or output from a flow simulation is available, similarity formulations are used. Essentially, the formulations employed are those from Rotach *et al.* (1996). However a revised formulation is used for the profile of Reynolds stress. In a near-neutral boundary layer, the Reynolds stress profile has been parametrized by Brost *et al.* (1982) as:

$$\overline{u'w'}(z) = -u_*^2 \left(1 - \frac{z}{z_i}\right), \tag{16}$$

where from now on the overbar stands for an average over time; u_* is the friction velocity. For stable conditions it has been parametrized by Nieuwstadt (1984) as:

$$\overline{u'w'}(z) = -u_*^2 \left(1 - \frac{z}{z_i}\right)^{3/2}, \tag{17}$$

where z_i is used for the mixing layer height of the convective boundary layer as well as for the depth of the stable boundary layer. Rotach *et al.* (1996) have slightly modified Eq. (16) in order to obtain an approximately constant Reynolds stress within the surface layer. (This can be desirable when focusing on dispersion problems within the surface layer or close to the surface. In such cases the 'constant-flux assumption' is then consistent with the more general Reynolds stress parametrization.) Here, a minor modification to their formulation is proposed, which allows it to cover both the unstable (Eq. 16) and stable (Eq. 17) boundary layer:

$$\overline{u'w'}(z) = -u_*^2 \left(1 - \frac{z}{z_i}\right)^a \Psi, \tag{18}$$

where:

$$\Psi^{-1} = \text{logit}(\xi) + \{1 - \text{logit}(\xi)\} \left(1 - \frac{z}{z_i}\right)^a, \tag{19}$$

with $a = 1$ for near-neutral conditions, $a = 3/2$ in a stable boundary layer, $0.1\xi = \sqrt{z/z_i} - 0.5$ and

$$\text{logit}(\xi) = \frac{\exp(\xi)}{1 + \exp(\xi)}. \tag{20}$$

The function Ψ alters the original parametrizations, Eqs. (16) and (17), only slightly in the region of the surface layer, where the value of $\overline{u'w'}(z)$ becomes approximately constant and asymptotically approaches $-u_*^2$ near the ground.

3. Reduction of the large-scale contribution as puff sizes grow

The particle part of the PPM represents the contributions for the whole turbulence energy spectrum. However, the relative diffusion in the puff part of the PPM already accounts for the effects of all eddies smaller than, or equal to, the puff size. With this, the total dispersion is overestimated more and more as the travel time increases, leading to underestimated ground-level concentrations far away from the source.

The procedure to circumvent this problem in the PPM is very simple: the turbulent velocities of the individual particles as calculated by the particle part of the model are smoothed, so that they only take into account the low-frequency part of the spectrum. The stochastic movement of the puff's centre is then based on these smoothed turbulent velocities. This approach is more accurate than smoothing the particle trajectories directly. This would prevent puff trajectories from closely approaching either the ground or the upper model-boundary, since particles are reflected there, and a smoothed trajectory will thus never reach these reflecting boundaries. When smoothing the turbulent velocities instead, the puff centres will still be well mixed all over the boundary layer as soon as the particles positions are well mixed.

To calculate the amount of dispersion which has to be 'smoothed away', the proportion of relative to absolute dispersion is calculated by means of the energy spectra. This proportion depends on the Lagrangian properties along the trajectory of the centre of the puff. Using Taylor's frozen-turbulence hypothesis, a frequency $n^*_{x,y,z} = \bar{u}(t)/(2\sigma_{x,y,z})$ for each direction is defined from the actual puff sizes σ_x, σ_y, σ_z (i.e. the standard deviations).

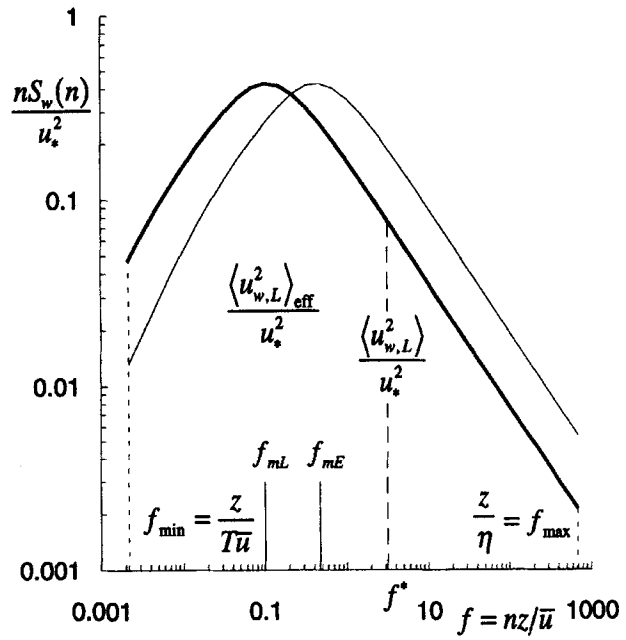

Figure 3. Determination of the ratio of turbulent eddies larger than the puff size, example for the vertical velocity component. The spectral density corresponds to a surface-layer formulation of Højstrup (1981), with $L = -10$ and $z_i = 1000$ m. The thin line shows the Eulerian spectrum, and the thick line the derived Lagrangian spectrum. The frequencies where their peaks occur are denoted as f_{mE} and f_{mL}, respectively. See text for further definitions and explanation.

We denote the integral over the low-frequency part of the Lagrangian energy spectrum as $\langle u_i^2 \rangle_{\text{eff}}$ ($i = u, v, w$), where $\langle u_i^2 \rangle_{\text{eff}} = \int_{n_{\min}}^{n_i^*} S_i \, \mathrm{d}n$, where S_i is the Lagrangian spectral density. Then, the ratio $r_i = \langle u_i^2 \rangle_{\text{eff}} / \langle u_i^2 \rangle$ is determined (Fig. 3). The integration of the whole spectrum runs from $n_{\max} = \bar{u}/\eta$, where $\eta = (\nu^3/\varepsilon)^{1/4}$ is the Kolmogorov micro-scale, ν is the kinematic molecular viscosity and ε as before is the dissipation rate, to $n_{\min} = 1/T$, where T is the averaging time for the measurements of the properties of the flow field, i.e. $\langle u_i^2 \rangle = \int_{n_{\min}}^{n_{\max}} S_i \, \mathrm{d}n$. This ratio r_i denotes the amount of dispersion which is not covered by relative dispersion.

To filter out the effect of the high-frequency part of the energy spectrum (i.e. the small eddies), a smoothing procedure over time is applied. The time series of stochastic turbulent velocity components of each particle is smoothed by use of a procedure with the effect of a low-pass filter. The trajectory of the centre of mass of the puffs is then calculated based on the time series of these smoothed turbulent velocities.

As the smoothing procedure, a Kalman filter is applied (see de Haan and Rotach 1997 for more details on Kalman filtering). This filtering technique is normally used to filter a 'true' value out of a noisy signal. It is especially suited, however, to smooth time series from stochastic processes. A traditional running mean, smoother for any instant of the time series, would rely on both past and future values (which are not yet known within stochastic processes), and requires all these values to be stored in the model (necessitating a huge storage capacity, as many values for thousands of three-dimensional trajectories are to be smoothed). The Kalman filter makes use of the fact that the order and the basic parameter of the underlying stochastic process of the particle model are known (an AR(1)

Figure 4. Example of smoothing of the time series of the turbulent velocity (u') as calculated by the particle model (solid line) with a Kalman filter (dashed line). The envelope (dotted lines) marks the interval $u'(t) \pm \tau(\sigma_x)$. Conditions of forced convection ($u_* = 0.4$ m s^{-1}, $L = -50$ m, $z_i = 2000$ m, $\bar{u} = 3.4$ m s^{-1}) are used for this example. See text for definitions and further explanation.

process, see section 2(c)), and for any time step it depends only on the smoothed value at the previous time step.

The amount of smoothing depends on the so-called 'window width', τ. It is chosen to be zero as $r_i = 1$ (i.e. for a very small puff the particle velocities are not smoothed at all). For large puffs $r_i \to 0$, and accordingly $\tau \to \infty$ is used in the PPM; thus the smoothing increases as the puffs grow. The ratios r_i are evaluated for each puff individually. As long as the puff sizes are small, the r_i will remain close to unity. Thus the turbulent velocities of the centres of the puffs within the PPM will closely resemble those of the particles (Fig. 4). As puff size grows, the values of the r_i decrease and eventually approach zero, leading to only minor turbulent movements of the puff centres. This allows the particle model within the PPM to be switched off as soon as r_i equals zero, then moving the puff centres with the average flow field only. For far-field concentration predictions, this causes considerable computational savings. Even when averaged over T, the velocity fluctuation of a stochastic process will not give exactly zero. Therefore, to ensure that the smoothed turbulent velocities approach zero as $r_i \to 0$, the smoothed values are multiplied by the factor $[0.5 \sin\{\pi(r_i - 0.5)\} + 0.5]$. Figure 4 depicts this procedure of smoothing the time series of the particle turbulent velocities, as calculated by the particle part of the model. More details about the application of a Kalman filter to remove the relative dispersion from particle velocities which account for absolute dispersion can be found in de Haan and Rotach (1997).

The literature about the form of Lagrangian velocity spectra is very sparse. Generally, it is assumed that the spectra show the same form as measured Eulerian fixed-point spectra, but are shifted towards lower frequencies by a factor $\beta = f_{mE}/f_{mL}$, where the non-dimensional frequency ($f = nz/\bar{u}$) where the maximum of the spectrum occurs is denoted by f_{mE} and f_{mL} for the Eulerian and Lagrangian spectra, respectively (see Fig. 3). Pasquill and Smith (1983; pp. 80–87) give as the best estimate from several different mea-

surements $\beta i \approx 0.6$, where $i = \sigma_u/\bar{u}$ is the turbulence intensity. In the PPM, an additional upper limit of 4 is assumed for β under weak turbulence conditions, which is supported by the measurements reported by Pasquill and Smith (1983; their Fig. 2.19).

Models of Eulerian velocity spectra are then taken from Højstrup (1981) for the unstable surface layer, and Højstrup (1982) for the unstable planetary boundary layer. The model of Kaimal *et al.* (1972) is used for the neutrally stratified surface layer. For the stable surface layer, the model of Olesen *et al.* (1984) is adopted. For the upper part of the neutral and of the stable boundary layers, no parametrizations for the velocity spectra can be found in the literature. In the present work, the same formulations as for the surface layer are used. Each of the above models is either given as an expression of the form $C(1 + Df^{5/3})^{-1}$ or as $A_1(1 + B_1 f)^{-5/3}$, or as a sum of both forms. To allow for an analytical integration between the boundaries $f_{\min}$, f^* and $f_{\max}$, the models of the form $C(1 + Df^{5/3})^{-1}$ are transformed into the form $A_2(1 + B_2 f)^{-5/3}$ by use of the transformations $B_2 = 1.5^{2/5} D^{3/5}$ and $A_2 = (3.1/1.5)^{3/5} C$. This ensures that the position of the maximum and the total integral are conserved. These transformations modify the spectrum from a 'pointed' to a more 'blunted' shape. $nS_i(n)$ becomes larger for small and large n, and its maximum value decreases. In the present work, $nS_i(n)$ is only used to calculate r_i. The change in r_i caused by the above transformations depends on the spectral model used. The maximum decrease in r_i occurs for $f \approx 0.1$ (and is about -12% in the most extreme case, where the original spectrum only consists of an expression of the form $C(1 + Df^{5/3})^{-1}$), and the maximum increase occurs at $f \approx 10$ ($+14\%$).

The approach outlined in this section aims at letting the dispersion in the puff part and in the particle part of the model sum to 100%. Yamada and Bunker (1988) report that their RAPTAD model yields best results when their full particle model is used together with Gaussian-shaped density estimators (e.g. puffs). These puffs are applied to each particle position, and enable the model to produce much smoother concentration fields as compared to the box-counting of particles. To determine the standard deviations of the puffs, absolute diffusion is used (Eq. (5)). Yamada and Bunker (1988) investigated the effect of reducing the amount of dispersion in the particle and puff parts of their model. They found that using the full particle model and absolute diffusion for the puffs yields better results as compared to enforcing the diffusion of the particle and puff parts of the model to sum up to 100%. It appears that they reduced the dispersion of both model parts with constant factors, not depending on the size of the puff. It is clear that the combination of a full particle model with absolutely dispersed puffs theoretically leads to an overestimation of dispersion. The good results reported by Yamada and Bunker might be explained by the fact that they apply their combined model to distances of 10 to 20 km from the source, i.e. clearly in the far-field limit. In this limit, relative and absolute dispersion differ from one another only marginally (see Fig. 2). Thus it becomes evident from the above considerations that the puff part of the model is expected to account for almost 100% of the total dispersion, and in the far-field limit the question whether relative or absolute dispersion is used is of no importance. As soon as puff dispersion has a larger effect than particle dispersion, the latter will hardly influence the resulting concentration distribution. This is illustrated by the fact that Yamada and Bunker mention that the amount of dispersion covered by the particle model is rather insensitive, and that correct concentration distributions are yielded as long as the puffs use full absolute dispersion (which equals relative diffusion in the far-field limit), and are not reduced by multiplication by a constant factor. Hence, for mesoscale applications as in Yamada and Bunker (1988), the particle part could actually be switched off (only regarding the dispersion; an advanced particle model with skewed pdf would still be needed to cope with convective conditions). For mesoscale applications, the additional dispersion caused by the particle model is unlikely to influence the results.

For the intermediate field (as defined in section 2(b)), however, this approach will yield better results if the dispersion covered by the puff and particle part of any combined model sums to 100%, where the relation between the two parts depends on the puff size.

4. Validation

(a) *Model validation experiments*

Due to the very limited amount of suitable experimental data on spatially inhomogeneous dispersion events, for which the PPM has been designed, this first validation is performed using tracer data from simpler flow configurations. The data sets used to validate the PPM are all from tracer experiments over flat terrain with a roughness length which is assumed to be constant, and without any information provided concerning the variation of the wind during the individual hours of measurement.

In a series of workshops aimed at harmonising short-range dispersion models in Europe (Olesen and Mikkelsen 1992; Cuvelier 1994; Kretzschmar *et al.* 1994; Kretzschmar and Cosemans 1996) three 'reference data sets' were defined for model comparison (Olesen 1995a).

From the Copenhagen tracer experiment, data from 9 hours of measurements under conditions of forced convection are available. The tracer was released at a height of 115 m, over a suburban surface. For the experiments in Lillestrøm, strongly stable winter conditions prevailed during the 8 observational periods of 15 minutes each. The experiment took place in a suburban environment, with a release height of 36 m. In the Kincaid tracer experiment, convective conditions were observed during most of the 171 hours of measurements within the present data set. The tracer was injected into the exhaust gases of a power plant situated in a rural environment at a height of 187 m. This short overview of the tracer experiments shows that these data sets represent a wide range of atmospheric stability conditions, and are suited for model validation. More details about the tracer experiments can be found in Gryning and Lyck (1984) for Copenhagen, Haugsbakk and Tønnesen (1989) for Lillestrøm and Bowne and Londergan (1983) for Kincaid. For the present validation, all runs of these three experiments have been simulated, except for the Lillestrøm data set where u_* was recorded as zero during one of the runs, a condition which the PPM cannot handle.

In all three tracer experiments, the receptors were placed on several arcs downwind of the source, and hourly (Lillestrøm: quarter-hourly) average measurements of the tracer concentrations were made at 2 m above ground. The mean wind speed was measured at different levels. For Kincaid, values for u_* and Obukhov length, L, are based on the meteorological pre-processor of Hanna and Paine (1989). Mixing-depth estimates come from several daily radiosonde soundings. For Copenhagen u_* and L were determined using a method identical to the one given in Hanna and Paine (1989). The mixing height is based on a daily radio sounding. In Lillestrøm, u_* and L were determined from sonic anemometer measurements at 10 m height. No mixing-depth information is available.

Additionally, for the Copenhagen and Lillestrøm data sets, measurements of the velocity statistics, $\langle u_2^2 \rangle$ and $\langle u_3^2 \rangle$, are available (those for the Kincaid experiment are generally considered to be unreliable). The releases in Copenhagen and Lillestrøm were non-buoyant, whereas at Kincaid a very strong plume rise (with vertical exit velocities in the range of 10–13 m s^{-1} and a temperature excess of over 100 deg C) has to be taken into account.

In general, in Copenhagen and Lillestrøm the measured concentration patterns on the arcs (i.e. the cross-wind contribution) exhibit more or less Gaussian shapes. Therefore, even Gaussian plume models can be expected to yield realistic results, although some meandering in Lillestrøm seems to have occurred. On the other hand, the concentration

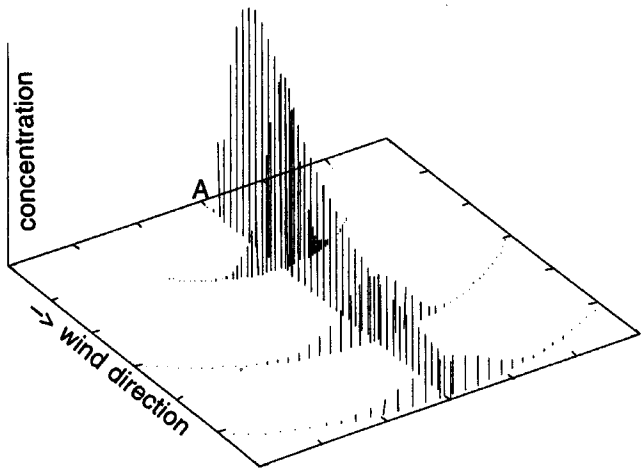

Figure 5. Simulated ground-level concentrations for the Copenhagen tracer experiment (run from 30 April 1979). The source location is indicated by 'A'. The concentration values are displayed at three virtual receptor arcs at 2, 4.2 and 5.9 km downwind from the source and in the plume centre line.

patterns observed on the receptor positions in Kincaid indicate that, owing to the convective conditions and possibly wind shear, the continuous plume release is torn into pieces. The lateral concentration pattern is very irregular in almost all the experiments.

(*b*) *Validation set-up*

The scaling parameters provided with the data sets (u_*, L, z_i) are used as model input. Where measurements of $\langle u_2^2 \rangle$ and $\langle u_3^2 \rangle$ were available (Copenhagen and Lillestrøm), the parametrized profiles were scaled (i.e. multiplied by the same constant for all heights) in order to match the measured values. The simulations are performed essentially by rebuilding the experimental set-up. Figure 5 depicts an example of the placement of the simulated receptors on 3 arcs and in the plume centre line. At the mixing height as well as at the ground, perfect reflection without any deposition of pollutants is assumed. For the Gaussian concentration distribution belonging to each puff, six image sources are assumed at $z = -h_s$, $2z_i - h_s$, $-2z_i - h_s$, $4z_i - h_s$ etc., where h_s is the actual height of the puff's centre. In the case of the Lillestrøm experiments, the height of the stable boundary layer, which had not been measured, is determined according to $z_i = d\sqrt{u_* L / f_c}$, with $d = 0.28$ (Stull 1988). To ensure that the inverse of the time steps for the simulation lies in the inertial subrange for the particle part of the model, the criteria following Rotach *et al.* (1996) are applied.

The mean wind profile was determined based on an approach from Sorbjan (see Rotach *et al.* (1996) for details) and has been scaled to minimise the sum of squared differences from the measurements. From the predicted concentrations at the individual receptors, the arcwise maximum concentration, the standard deviation of the concentration distribution on the arc and the cross-wind integrated concentration (on the arc) are determined.

(*c*) *Results*

As statistical measures to describe the model performance, the fractional bias, $FB = (\bar{C}'_{\text{obs.}} - \bar{C}'_{\text{pred.}})/\{0.5(\bar{C}'_{\text{obs.}} + \bar{C}'_{\text{pred.}})\}$, the normalised mean square error, $NMSE = \overline{(C'_{\text{obs.}} - C'_{\text{pred.}})^2}/(\bar{C}'_{\text{obs.}}\bar{C}'_{\text{pred.}})$, and the correlation coefficient, $COR =$

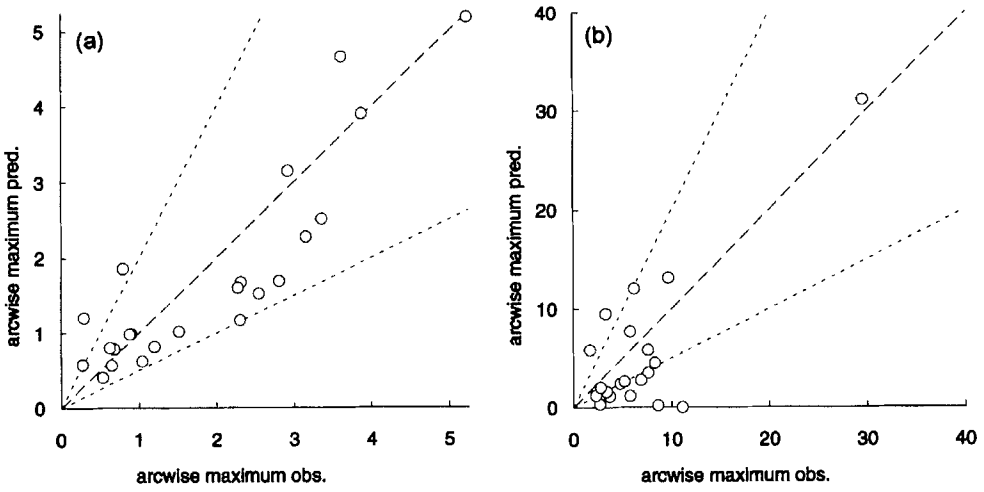

Figure 6. Scatter plots of the observed (obs.) and predicted (pred.) PPM arcwise maximum tracer concentrations for (a) the Copenhagen and (b) the Lillestrøm tracer experiments. The dashed lines mark the area within which a predicted value lies within a factor of 2 of the observed value. Units are $\mu g\ m^{-3}$.

$(C'_{obs.} - \bar{C}'_{obs.})(C'_{pred.} - \bar{C}'_{pred.})/(\sigma_{obs.}\sigma_{pred.})$ are determined; $C'_{obs.}$ is the normalised observed concentration, $C'_{obs.} = C_{obs.}/Q$ where Q denotes the source strength; $C'_{pred.}$ is the simulated concentration, and $\sigma_{obs.}$ and $\sigma_{pred.}$ are the respective standard deviations. Confidence limits have been calculated using the seductive blockwise bootstrap resampling method proposed by Hanna (1989). 1000 samples from $C'_{obs.} - C'_{pred.}$ pairs are taken, and 95% confidence limits are based on the 2.5% and 97.5% quintiles of the distribution of statistics for the 1000 samples (so-called bootstrap-percentile confidence intervals).

(i) *Copenhagen.* The simulated results for the Copenhagen experiment show, in general, a good correspondence to the observations (Fig. 6(a)). Since the receptors during the Copenhagen experiment seem to have missed the concentration maximum, which occurred closer to the source than the closest receptor, no conclusion can be drawn concerning the ability of the PPM to predict the maximum surface concentration. Figure 6(a) shows the comparison of the observed and predicted arcwise maximum concentrations. Only two predicted values differ from the observation by more than a factor of 2. These data points belong to the only experimental run for which the parametrized profile of wind fluctuation standard deviations had to be multiplied by a high factor, in order to let the profile match the measured value (see section 4(b)). On average, a small underprediction of the arcwise maximum (*ArcMax*) and a more pronounced underprediction of the cross-wind integrated concentration (*CIC*) can be observed (positive *FB* in Fig. 8). The underprediction is significantly different from zero, on a 95% level for *CIC* (i.e. the confidence limits do not include zero). The correlation is remarkably high for *ArcMax* and somewhat lower for *CIC*. The scatter (i.e. the *NMSE*) is rather low for the predicted *ArcMax* and, as for the *FB*, higher for the *CIC*, and differs from zero on a 95% level in both cases.

The results of using the Lagrangian particle dispersion model (LPDM) of Rotach *et al.* (1996) alone (which constitutes the particle part of the PPM) are also shown in Fig. 8 for *CIC*. For the Copenhagen data set the PPM performs only slightly worse than the full particle model, indicating that the approximation of a number of particles as a puff (according to the second interpretation of the PPM concept in section 2(a)) does not

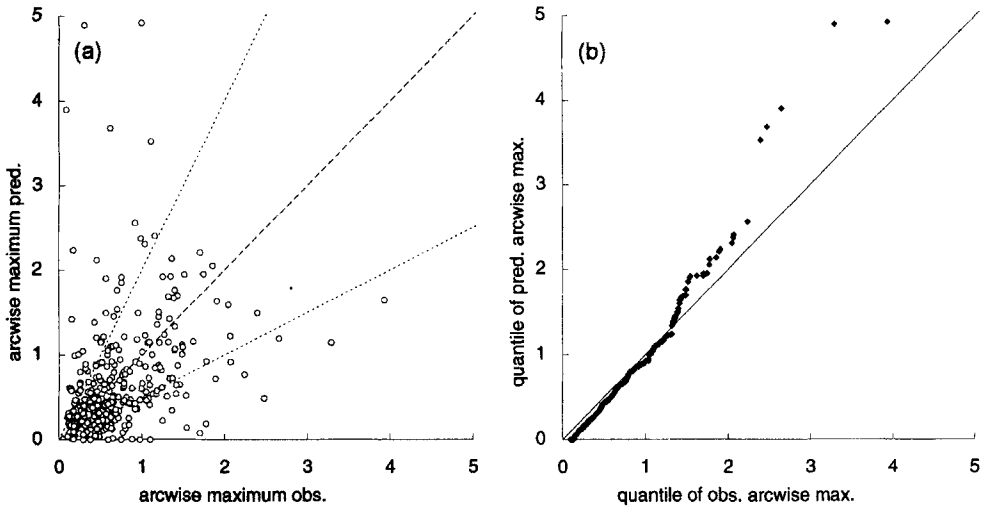

Figure 7. (a) Scatter plot and (b) quantile–quantile plot of observed (obs.) and predicted (pred.) arcwise maximum concentrations for the Kincaid tracer experiment. Units are $\mu g\ m^{-3}$.

lead to a much worse performance, while additionally providing information on the lateral concentration distribution.

(ii) *Lillestrøm.* For the Lillestrøm experiment, the results for the *ArcMax* are encouraging (Fig. 6(b)). Regarding the difficult dispersion regime, the $NMSE$ of below unity (see Fig. 9) can be regarded as satisfying. Note however, that a single data point (see Fig. 6(b)) has a very strong influence on these statistical measures. This leads to very large confidence limits. For two succeeding observational periods with a very small Obukhov length (12 January 1987), the PPM predicts the maximum concentration far away from the source, while the measurements indicate a well-defined maximum close to the source as for the other episodes (not shown). Therefore, the CIC is underpredicted by roughly 30% on average, with the most severe underpredictions for the arc closest to the source. The underprediction of the *ArcMax* is lower and not significantly different from zero on a 95% level. Compared to the LPDM, the PPM even performs slightly better in $NMSE$ and COR.

(iii) *Kincaid.* The release during the Kincaid experiment was highly buoyant. The effective plume height has been parametrized using the formulae of Briggs (1984) (for all models compared in section 4(d)). Figure 7(a) depicts a scatter plot of the results for the Kincaid experiment. For the present validation, those hours of measurements tagged as 'quality 3' (Olesen 1995a) have been selected. This highest-quality tag indicates that a clearly defined maximum concentration could be identified on the receptor arcs. The quality-3 subset contains a total of 338 receptor arc measurements. Considering the patchy concentration patterns observed during the Kincaid campaign, plume models not suited for convective conditions will tend to fail. Advanced particle models based on a skewed probability function are expected to yield better results. The same holds true for the PPM since it uses a particle model allowing for a convective pdf (section 2(c)). Because of the stochastic nature of the experimental data, no model can be expected to be able to predict to a good correspondence the spatial and time-dependent concentration distribution. But the distribution of predictions should resemble the distribution of the measurements. Therefore, and since the number of observations is much larger than for the two other experiments, a quantile–quantile plot is shown in Fig. 7(b). The agreement between the distribution

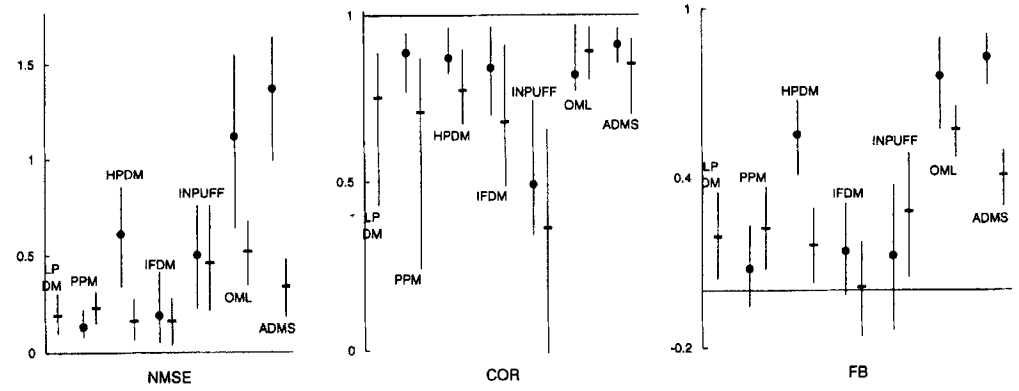

Figure 8. Comparison of results from the Copenhagen experiment. NMSE (normalised mean square error), COR (correlation coefficient) and FB (fractional bias) for arcwise maximum *ArcMax* (dots), and cross-wind integrated concentration CIC (minus sign) for 23 observations for the Puff–Particle Model (PPM) and other models. The vertical lines show the 95% confidence limits calculated with bootstrap resampling. The horizontal lines depict the values for a perfect model (NMSE and FB: 0, COR: 1). Data for the other models is taken from Olesen 1995b. For the full titles of the other models see text.

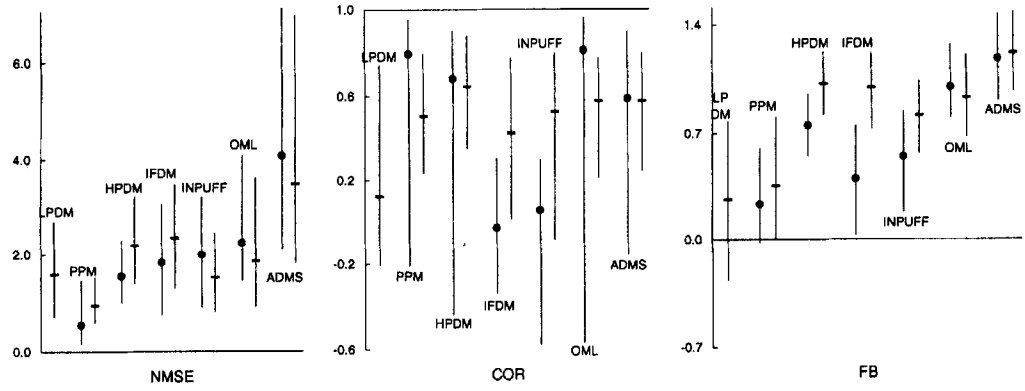

Figure 9. As Fig. 8 but for the Lillestrøm experiment and for 20 observations.

of predicted and observed *ArcMax* appears to be very good, with a slight tendency for overprediction towards high concentration values.

No reliable measurements of the CIC are available for the Kincaid data set. The underprediction by the PPM of the *ArcMax* is modest and not significantly different from zero (Fig. 10). The correlation of approximately 0.4 is also considered to be a very good result with respect to very irregular concentration patterns. The latter, of course, is responsible for the value of the $NMSE$ close to unity. In general, the fact that this data set consists of 338 data points leads to more precise estimates of the model performance than depicted by the other statistical measures discussed in this section. This becomes evident from the confidence limits which are generally smaller than those shown in Figs. 8 and 9 (see Fig. 10).

(*d*) *Comparison with other models*

The results for the simulations with the PPM and the LPDM are also compared with those of five other dispersion models. These are the HPDM-4 (Hybrid Plume Disper-

sion Model; Hanna and Chang 1993), the Danish OML (Operationalske Modeller om Luftforureninger; Olesen *et al.* 1992), the IFDM (Immission and Frequency Distribution Model; Cosemans *et al.* 1992), INPUFF (Integrated Puff dispersion model; Sandu 1995), and UK-ADMS (Atmospheric Dispersion Modelling System: Carruthers *et al.* 1992). The OML and UK-ADMS are new-generation Gaussian plume models, whereas IFDM and INPUFF are a Gaussian plume and puff model, respectively, depending on stability classes, and the HPDM is a new-generation hybrid model consisting of four sub-models for different atmospheric stability regimes. For the Copenhagen and the Lillestrøm data set, all models except the OML used the measured values of $\langle u_2^2 \rangle$ and $\langle u_3^2 \rangle$. For the model intercomparison, 95% confidence intervals are estimated on the differences in FB and $NMSE$ between each pair of models, using the bootstrap resampling (Hanna 1989). Models are considered as having different performance only if their FB and/or NMSE are different on a 95% level. While comparing the performance of the PPM and the LPDM with the other models, it should be kept in mind that the PPM requires much greater (roughly 2 orders of magnitude) computational time than models solving plume equations analytically, and the LPDM even needs a further factor of ten times more CPU time than the PPM.

All models, including the PPM and the LPDM, underpredict the surface concentrations for the Copenhagen data set (positive FB, Fig. 8). This has been attributed by Rotach and de Haan (1997) to the influence of the rough urban character of the underlying surface, which leads to the formation of an urban roughness sublayer. Using the LPDM, Rotach and de Haan (1997) have shown, that this underprediction can be resolved when the turbulence and flow structure of an urban roughness sublayer is explicitly taken into account. The performance of the IFDM model, which relies on stability classes, is remarkable. Most models perform better in predicting the CIC than the *ArcMax* (this is most pronounced for the ADMS and OML models, which have severe difficulties predicting the *ArcMax* but clearly perform better on the CIC). The correlation coefficient is generally very high, with the values of the INPUFF model being lowest. Comparing the models, the performance of the PPM is significantly better than that of the HPDM, OML and ADMS, regarding the FB and $NMSE$. Concerning COR, the PPM differs significantly only from the INPUFF model. For CIC, the PPM can only be said to be significantly better than the OML (regarding $NMSE$ and FB) and the ADMS and IFDM (FB).

For Lillestrøm, all models perform worse in terms of the given statistical measures than for the Copenhagen data set. Generally, large differences can be detected between the individual models (Fig. 9). For all the experiments in Lillestrøm, the sun was at a very low angle (they were started only 15 minutes after sunrise on average). Furthermore, no stable boundary layer heights were observed (a ground-based inversion was present). The INPUFF and IFDM models do not require a mixing depth as input; the LPDM, HPDM, PPM and ADMS use the parametrization given in section 4(b), where the ADMS assumes a minimum value of 50 m (Carruthers 1997, personal communication). The OML assumed the mixing depth to have a constant value of 200 m. These different parametrizations are likely to have a strong impact on the simulation results. Nevertheless, the results from the PPM seem to be encouraging compared to the other models (Fig. 9). The PPM has a smaller bias and scatter ($NMSE$) than all other models, and the smaller confidence limits (though still very large) also show up in a high COR value. Because of the very large confidence limits, differences between the PPM and other models for *ArcMax* are significant compared to HPDM, OML and ADMS (regarding $NMSE$ and FB). For CIC predictions, differences are significant for the HPDM and ADMS ($NMSE$) and to all models regarding FB.

For the Kincaid experiment the large differences in model performance, even between the three Gaussian plume models (Fig. 10), is partly due to the fact that some modellers

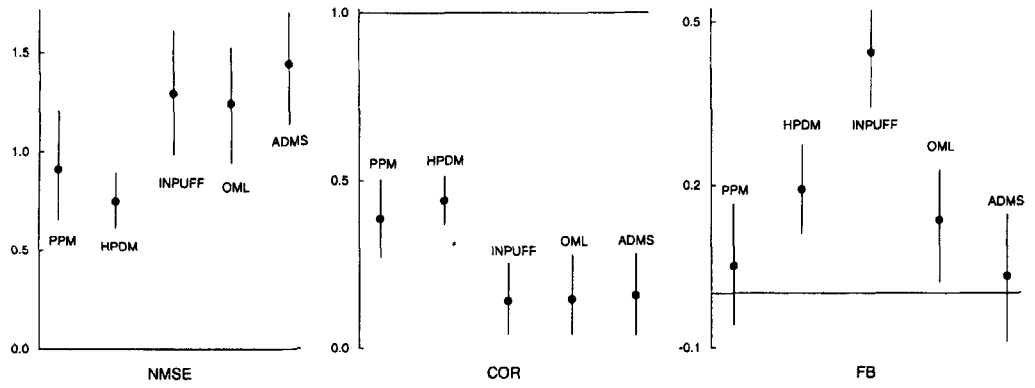

Figure 10. As Fig. 8 but for the Kincaid experiment and for 338 observations.

used the observed mixing height as an input parameter, whereas others used the results from a meteorological pre-processor. For the present simulations with the PPM, the predicted mixing heights after Hanna and Paine (1989) are used. The HPDM also used these predicted values, whereas the other models (i.e. OML and ADMS) used the observed values. For several non-zero observations, most of them measured after sun set, the PPM gives a prediction of zero. The PPM has a very low bias, not significantly different from zero, and a modest scatter ($NMSE$) and correlation. Overall, the PPM performs best, with similar $NMSE$ and COR as the HPDM (the second-best model), but with a significantly smaller FB. This is probably caused by the fact that the PPM is the only model using a convective pdf. The results for the Kincaid data set might be regarded as more valuable, because of the high number of observations allowing for a better model intercomparison.

5. Summary and conclusions

In the present paper, an approach to model dispersion is presented which aims at combining the advantages of puff models and particle models. The resulting model type is called Puff-Particle Model (PPM). In the PPM, a few hundred puffs are simulated in three-dimensional space, as compared to many thousand particles usually required in pure particle models. The concept of the PPM is very simple: while puff growth is described by the concept of relative dispersion (thus accounting for eddies smaller than the puff), the effect of meandering (i.e. the variation between the trajectories of different puffs) due to larger eddies (larger than the actual puff size) is simulated by introducing puff-centre trajectories derived from particle trajectories from a particle model. Thus, the PPM can be interpreted in two ways: first, compared to conventional Lagrangian particle models the PPM requires less computing time, not accompanied by a significant loss in accuracy; second, it can be regarded as a puff model for applications in which no frequently updated meteorological fields are available to resolve all eddies larger than the puffs. Thus, in the absence of frequently updated meteorological information, the PPM is able to give better predictions in the near-field compared to traditional puff models. If one puff trajectory is followed, this gives a single realisation of an instantaneous release, with the correct dispersion (relative diffusion). Averaging over, say, one thousand such realisations gives an appropriate picture of the additional effect caused by meandering, since the meandering effect of all those eddies larger than the puff, but not resolved by the flow field, is simulated using stochastic puff-centre trajectories, yielding the correct ensemble plume statistics.

The validation, using data from three different tracer experiments covering all atmospheric stability conditions, shows a good model performance for the prediction of both the maximum concentration on an arc of receptors (*ArcMax*) and the cross wind integrated concentration (CIC). In general, the predictions of the PPM have statistical measures which are better than those of other models.

The PPM allows for a correct description of dispersion, regardless of the updating frequency of flow field information, i.e. regardless of whether all large eddies are resolved by the flow field. This way, the modeller is not forced to choose between absolute dispersion (and only allowing for one flow field per, say, 60 minutes in order not to overestimate dispersion) on the one hand, and the use of relative diffusion on the other hand, with the effect of missing part of the dispersion, which will be most important for near- and intermediate-field concentration predictions. Instead, the modeller might use just as many flow field information updates as there are available.

The main fields of possible application of the PPM are those of conventional puff models, where the turbulence statistics of the flow field are sparse or infrequently provided. Additionally, the PPM has advantages for situations in which particle models have their strength (e.g. convective boundary layers, or in and above canopies), since it requires less computing time than the latter and at the same time offers the advantages of puff models, especially concerning the treatment of buoyant plume rise.

Acknowledgements

The present work was financed by the Swiss Federal Department of Education and Sciences (BBW) and the Swiss Agency of Environment, Forest and Landscape (BUWAL) through a project in the framework of COST 615 (citair). Thanks go to both reviewers for their many instrumental suggestions and for drawing our attention to the work of Hanna (1989).

References

Batchelor, G. K. 1952 Diffusion in a field of homogeneous turbulence—Part II: The relative motion of particles. *Proc. Camb. Philos. Soc.*, **48**, 345–362

Borgas, M. S. and Sawford, B. L. 1994 A family of stochastic models for two-particle dispersion in isotropic homogeneous stationary turbulence. *J. Fluid Mech.*, **279**, 69–99

Bowne, N. E. and Londergan, R. J. 1983 'Overview, results, and conclusions for the EPRI plume model validation and development project: Plains site'. EPRI report EA-3074, Electrical Power Research Institute, Palo Alto, USA

Briggs, G. A. 1984 Plume rise and buoyancy effects. In *Atmospheric science and power production*. Ed. D. Randerson. DOE/TIC 27601. Department of Commerce, Springfield, USA

Brost, R. A., Wyngaard, J. C. and Lenschow, D. H. 1982 Marine stratocumulus layers: Part II: Turbulence budgets. *J. Atmos. Sci.*, **39**, 818–836

Carruthers, D. J., Holroyd, R. J., Hunt, J. C. R., Weng, W.-S., Robins, A. G., Apsley, D. D., Smith, F. B., Thomson, D. J. and Hudson, B. 1992 UK atmospheric dispersion modelling system. In *Air pollution modelling and its applications IX*. Eds. H. van Dop, and G. Kallos. Plenum Press, New York, USA

Cosemans, G., Kretzschmar, J. and Maes, G. 1992 'The Belgian Immission Frequency Distribution Model'. Pp. 149–150 in Olesen, H. R. and Mikkelsen, T. q.v.

Cuvelier, C. (Ed.) 1994 Proceedings of the 2nd workshop on intercomparison of advanced practical short-range atmospheric dispersion models, 30 Aug.–3 Sept. 1993, Manno, Switzerland. Available from C. Cuvelier, JRC Ispra, TP 690, I-21020 Ispra (VA), Italy

Du, S., Sawford, B. L., Wilson, J. D. and Wilson, D. J. 1995 A determination of the Kolmogorov constant (C_0) for the Lagrangian velocity structure function, using a second-order Lagrangian stochastic model for decaying homogeneous, isotropic turbulence. *Phys. Fluids*, **1,** 3083–3090

Gryning, S.-E. and Lyck, E. 1984 Atmospheric dispersion from elevated sources in an urban area: Comparison between tracer experiments and model calculations. *J. Clim. Appl. Meteorol.*, **23,** 651–660

Gryning, S.-E., Holtslag, A. A. M., Irwin, J. S. and Sivertsen, B. 1987 Applied dispersion modelling based on meteorological scaling parameters. *Atmos. Environ.*, **21,** 79–89

de Haan, P. and Rotach, M. W. 1995 A puff-particle dispersion model. *Int. J. Environ. and Pollution*, **5,** Nos. 4–6, 350–359

de Haan, P. and Rotach, M. W. 1997 'The treatment of relative dispersion within a combined Puff-Particle Model (PPM)'. In Proceedings of the 22nd NATO/CCMS international technical meeting on air pollution modeling and its applications. Plenum Press, New York, USA

Hanna, S. R. 1989 Confidence limits for air quality model evaluations, as estimated by bootstrap and jackknife resampling methods. *Atmos. Environ.*, **23,** 1385–1398

Hanna, S. R. and Chang, J. C. 1993 Hybrid Plume Dispersion Model (HPDM) improvements and testing at three field sites. *Atmos. Environ.*, **27A,** 1491–1508

Hanna, S. R. and Paine, R. J. 1989 Hybrid Plume Dispersion Model (HPDM) development and evaluation. *J. Appl. Meteorol.*, **28,** 206–224

Haugsbakk, I. and Tønnesen, D. A. 1989 'Atmospheric dispersion experiments at Lillestrøm. 1986–1987'. Data Report NILU OR 41/89. Available from Norwegian Inst. for Air Research, PO Box 100, N-2007 Kjeller, Norway

Højstrup, J. 1981 A simple model for the adjustment of velocity spectra in unstable conditions downstream of an abrupt change in roughness and heat flux. *Boundary-Layer Meteorol.*, **21,** 341–356

1982 Velocity spectra in the unstable planetary boundary layer. *J. Atmos. Sci.*, **39,** 2239–2248

Hurley, P. J. 1994 Partpuff—A Lagrangian particle-puff approach for plume dispersion modelling applications. *J. Appl. Meteorol.*, **33,** 285–294

Hurley, P. and Physick, W. 1993 A skewed homogeneous Lagrangian particle model for convective conditions, *Atmos. Environ.*, **27A,** 619–624

Kaimal, J. C., Wyngard, J. C., Coté, O. R. and Izumi, Y. 1972 Spectral characteristics of surface layer turbulence. *Q. J. R. Meteorol. Soc.*, **98,** 563–589

Kretzschmar, J. G. and Cosemans, C. (Eds.) 1996 Pre-prints of the 4th workshop on harmonisation within atmospheric dispersion modelling for regulatory purposes. 6–9 May 1996. Oostende, Belgium. Available from J. Kretzschmar, VITO, Boeretang 200, B-2400 Mol, Belgium

Kretzschmar, J. G., Maes, G. and Cosemans, C. (Eds.) 1994 Pre-prints of the 3rd workshop on operational short-range atmospheric dispersion models for environmental impact assessment. 21–24 Nov. 1994, Mol, Belgium. Available from J. Kretzschmar, VITO, Boeretang 200, B-2400 Mol, Belgium

Luhar, A. K. and Britter, R. E. 1989 A random walk model for dispersion in inhomogeneous turbulence in a convective boundary layer. *Atmos. Environ.*, **23,** 1911–1924

Mikkelsen, T., and Larsen, S. E. 1984 Description of the Risø Puff Diffusion Model. *Nuclear Technol.*, **67,** 56–65

Mikkelsen, T., Larsen, S. E. and Pécseli, H. L. 1987 Diffusion of Gaussian puffs. *Q. J. R. Meteorol. Soc.*, **113,** 81–105

Nieuwstadt, F. T. M. 1984 The turbulent structure of the stable, nocturnal boundary layer. *J. Atmos. Sci.*, **41,** 2202–2216

Olesen, H. R. 1995a Data sets and protocol for model evaluation. *Int. J. Environ. and Pollution*, **5,** 693–701

1995b The model validation exercise at Mol: Overview of results. *Int. J. Environ. and Pollution*, **5,** 761–784

Olesen, H. R. and Mikkelsen, T. (Eds.) 1992 Proceedings of the 1st workshop on objectives for the next generation of practical short-range atmospheric dispersion models, 6–8 May 1992, Risø, Denmark. Available from H. Olesen, NERI, PO Box 358, DK-4000 Roskilde, Denmark

Olesen, H. R., Larsen, S. E. and Højstrup, J. 1984 Modelling velocity spectra in the lower part of the planetary boundary layer. *Boundary-Layer Meteorol.*, **29,** 285–312

Olesen, H. R., Løfstrøm, P., Berkowicz, R. and Jensen, A. B.	1992	An improved dispersion model for regulatory use: the OML model. In *Air pollution modelling and its applications IX*. Eds. H. van Dop and G. Kalles. Plenum Press, New York, USA
Pasquill, F. and Smith, F. B.	1983	*Atmospheric Diffusion, 3rd edition*. John Wiley & Sons, New York, USA
Richardson, L. F.	1926	Atmospheric diffusion shown on a distance-neighbour graph, *Proc. R. Soc.*, London A, **110,** 709–737
Rotach, M. W.	1995	'The universal constant of the Lagrangian structure function: Its effect on dispersion characteristics under varying stability'. Pp. 289–292 in Pre-prints 11th symposium on boundary layers and turbulence. Charlotte. American Meteorological Society, Boston, USA
Rotach, M. W. and de Haan, P.	1997	On the urban aspect of the Copenhagen data set. *Int. J. Environ. Pollution*, **8,** 279–286
Rotach, M. W., Gryning, S.-E. and Tassone, C.	1996	A two-dimensional stochastic Lagrangian dispersion model for daytime conditions. *Q. J. R. Meteorol. Soc.*, **122,** 367–389
Sandu, I.	1995	Evaluation of the Gaussian puff model based on measurements. *Int. J. Environ. and Pollution*, **5,** 375–381
Scire, J. S., Strimaitis, D. G., Yamartino, R. J. and Zhang, X.	1995	A user's guide for the CALPUFF dispersion model. Prepared for the USDA Forest Service, Cadillac MI, by Earth Tech, Inc., Concord, USA
Smith, F. B. and Hay, J. S.	1961	The expansion of clusters of particles in the atmosphere. *Q. J. R. Meteorol. Soc.*, **87,** 82–101
Stull, R. B.	1988	*An introduction to boundary layer meteorology*. Kluwer Academic Publishers, Dordrecht, The Netherlands
Taylor, G. I.	1921	Diffusion by continuous movements. *Proc. London Math. Soc.*, Ser. 2, **20,** 196–211
Thomson, D. J.	1987	Criteria for the selection of stochastic models of particle trajectories in turbulent flows. *J. Fluid Mech.*, **180,** 529–556
Thykier-Nielsen, S., Mikkelsen, T., Larsen, S.-E., Troen, I., de Baas, A. F., Kamada, R., Skupniewicz, C. and Schacher, G.	1989	'A model for accidental releases in complex terrain'. In: *Air pollution and its application VII*. Ed. H. van Dop, Plenum Press, New York, USA
Thykier-Nielsen, S., Mikkelsen, T. and Santabàrbara, J. M.	1994	'Experimental evaluation of a PC-based real-time dispersion modelling system for accidental releases in complex terrain'. Pp. 383–394 in *Air pollution and its application X*. Eds. S.-E. Gryning and M. M. Millán. Plenum Press, New York, USA
Wilson, J. D. and Sawford, B. L.	1996	Review of Lagrangian stochastic models for trajectories in the turbulent atmosphere. *Boundary-Layer Meteorol.*, **78,** 191–210
Yamada, T. and Bunker, S.	1988	Development of a nested grid, second moment turbulence closure model and application to the 1982 ASCOT Brush Creek data simulation. *J. Appl. Meteorol.*, **27,** 562–578